International Journal of Concrete Structures and Materials

RESEARCH Open Access

The Behavior of Post-installed Rebar Connectors in Steel Frame Retrofitted Concrete Structures Under Combined Shear and Tension

Rong Zeng[1,2], En-He Bao[1,2], Xia Yin[1,2] and Feng Fu[3*]

Abstract

To investigate the response of post-installed rebar connectors in steel frame retrofitted concrete structures under combined shear and tension, seven shear-and-tensile tests were conducted. The bearing capacity, stiffness, and hysteresis behavior of the connectors were investigated during the tests. Both Monotonic and cyclic load regimes were applied in the loading process. The results show that with the increase of the loading angle, the deformation capacity, the yield force, ultimate tensile force, and tensile stiffness of the specimen decrease, while the maximum shear force and shear stiffness of the specimen increase. The bearing capacity, stiffness, and energy dissipation performance of the specimen under a monotonic load is greater than that under the coupled shear-and-pull load. The bearing capacity, stiffness, hysteresis curve, and failure status of the specimens are not affected by different loading regimes. At the end, the design formula of anchor bolt for this type of connectors from the design code of China, United States, and Japan were compared. Formulas to calculate the shear strength under combined shear and tension is developed.

Keywords Post-installed rebar connector, Shear performance, Deformation, Strength, Equivalent shear capacity, Equivalent tensile capacity

1 Introduction

In 2008 Wenchuan earthquake, various damages to buildings within 50 kM of the epicentre were observed, including the RC structures built after 2002 (Civil & Structural Groups of Tsinghua University, Xian Jiaotong University and Beijing Jiaotong University, 2008), (Ministry of Housing & Urban-Rural Development, 2010). Therefore, it is necessary to retrofit the existing RC structures which have insufficient ability to resist the seismic load.

There are many technical specifications for the design, construction of post-installed anchor connectors of concrete structures from various countries (ACI318—11, 2013; Design Recommendations for Composite Constructions, 2010; Ministry of Housing & Urban-Rural Development, 2013). The single-sided anchor connectors are widely used in retrofitting concrete structures because it has the advantages of simple construction, fast and reliable anchorage, etc. (Cheng et al., 2017; Jianguo et al., 2014; Lee et al., 2010; Mourad, 1993; Mourad et al., 1996; Nie et al., 2015). Presently, numerous experimental studies of mechanical properties of the post-installed rebars under monotonic loading have been presented, such as: tensile tests (Liu et al., 2010; Xie et al., 2015; Yilmaz et al., 2013; Zhang et al., 2016), shear tests (Çalışkan et al., 2013; Ding et al., 2016; Gesoğlu

Journal information: ISSN 1976-0485 / eISSN 2234-1315.

*Correspondence:
Feng Fu
feng.fu.1@city.ac.uk
[1] Guangxi Key Laboratory of Green Building Materials and Construction Industrialization, Guilin University of Technology, Guilin 541004, China
[2] Guangxi Key Laboratory of Geomechanics and Geotechnical Engineering, Guilin University of Technology, Guilin 541004, China
[3] Department of Engineering, School of Science and Technology, City, University London, Northampton Square, London EC1V0HB, UK

et al., 2014; Xiaosong et al., 2018), compression–shear tests (Peng et al., 2018) and so on. Research on connectors used for structures, member connections and reinforcement were made in Cheng et al., (2017); Mourad (1993); Mourad et al., (1996). Among the anchor bolts for post-installed rebar connectors, reinforcement anchor is heavily used to repair concrete structures due to its advantages of simple construction, fast anchoring and reliability. (Ministry of Housing & Urban-Rural Development, 2010; Xiaosong et al., 2018; Yilmaz et al., 2013) carried out a number of experimental studies on the pull-out of the post-installed rebar. In Xie et al., (2015), Yilmaz embedded the post-installed rebar into low strength concrete specimens and studied the tensile performance of the connector with post-installed rebar using the diameter of the reinforcement, the anchorage depth and the distance from the centre of the reinforcement to the edge of the concrete substrate as analysis parameters.

However, for to steel frame retrofitted RC structure, as shown in Fig. 1a. The connectors between the RC structure and the new steel structure is made through some post-installed rebars as shown in Fig. 1b, causing combined shear and tension on the post-installed rebars. The layout details of the post-installed rebars specimens are shown in Fig. 1c. So far, little research on the effect of combined shear and tension on the post-installed rebars was made.

Therefore, in this paper, static and cyclic tests were performed to 7 groups of post-installed rebar connectors. The failure mode, bearing capacity and stiffness of each group of specimens were investigated in detail, formulas to calculate the shear strength under combined shear and tension is developed.

2 Test Setup

2.1 Test Specimens

Following the guidelines of Chinese code (JGJ145-2004) "Technical Specification for Post Anchorage of Concrete Structures" (Ministry of Housing & Urban-Rural Development, 2005), seven groups of post-installed rebars were tested under different loading methods. The diameter of the post-installed rebar was 20 mm, and the length of the post-installed rebars was 350 mm, with anchorage length of 260 mm by taking into account the shear forces limit. The effective anchorage is actually 240 mm due to 20 mm length of resection along 45° in the post-installed rebar, as shown in Fig. 2a. The construction sequence of retrofitting the reinforced concrete beams are: ① boring the hole with diameter of 25 mm, ② hole cleaning, ③ glue injection, ④ rebar embedment, and ⑤ curing of glue. The completed work is shown in Fig. 2b. In the experiment, the dimension of the RC beams was 400 mm × 400 mm × 1000 mm. HRB400 reinforced bars with diameters of 18 and 8 mm were used as the main reinforcement and stirrups, respectively, and concrete grade is C30. A steel plate with the thickness of 22 mm was placed between the RC beam and the post-installed rebar. The illustration of post-installed rebar and the loading plate on the RC beam, is shown in Fig. 2c, d.

Four loading angles (the angle between the post-installed bar and the load direction): 0° for pure tension, 90° for pure shear, 30° and 60° for shear–tension coupling effects, are chosen in this test. The fixed axial force ratio T/T_{u} of 0.7 was applied in the test, where T is axial tensile force, $T_u = A_S \times \sigma_{u,}$ A_{S} is the area of the post-installed rebar, and σ_u is the tensile strength of post-installed rebar. The test parameters of each group of specimens are shown in Table 1.

2.2 Material Properties

Table 2 shows the mechanical properties of the standard specimens of post-installed rebars from tensile test results.

2.3 Test Rigs

The illustration of the test rigs is shown in Fig. 3, similar test rigs can be found in Qian et al., (2020, 2021, 2022). The loading plates and the post-installed rebar are fixed to a RC beam, through 19 mm diameter bolts in the vertical direction, and the beam is anchored to the static base. The movement of the RC beam in the horizontal direction under the action of shear force was restrained with a steel bar with the diameter of 23 mm and Chinese steel angle section of L125X 12. The loading plate was connected to an L-shaped loading beam, where the tensile load was applied on through a vertical actuator connected to a guide rail, and the shear force was applied on through the horizontal actuator.

3 Loading Method and Instrumentation

3.1 Loading Method

Both monotonic loading and cyclic load regimes were applied on the load beam, respectively. For static load there are four different angles between the post-installed rebar and the load: 0°, 30°, 60° and 90°, where 0° is representing pure tension, and 90° is representing pure shear force. The cyclic load has been added with the angle of ± 1/500, ± 1/250, ± 1/125, ± 1/100 ~ ± 1/25.

The deformation is controlled after loading within the ranges of ± 0.2 mm, ± 0.4 mm, ± 0.8 mm, ± 1.0 mm, ± 1.5 mm, ± 2.0 mm, ± 2.5 mm, ± 3.0 mm, ± 3.5 mm, and ± 4.0 mm, respectively. Forward loading is continued until the component reaches the limit state which is considered that the component is damaged.

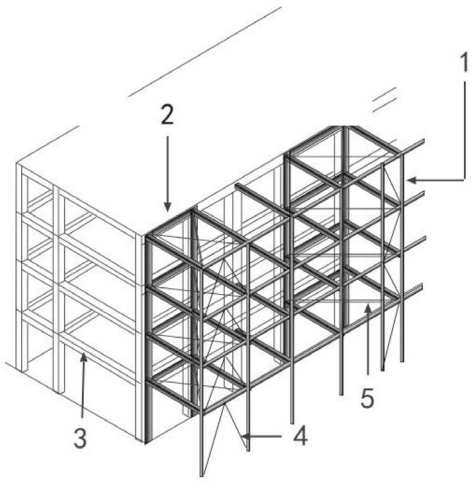

1—New steel frame structure
2—RC and steel structure anchorage joint
3—Built RC Frame
4—Vertical support
5—Horizontal support

(a) Retrofitting of a building

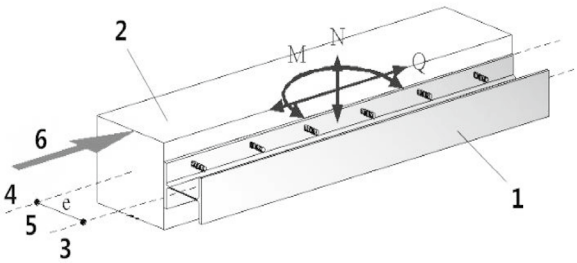

1—H steel beam of new steel frame structure
2—Built RC Frame Beams
3—H steel beam
4—RC beam 5—Eccentricity
6—Seismic force

(b) Anchorage joints

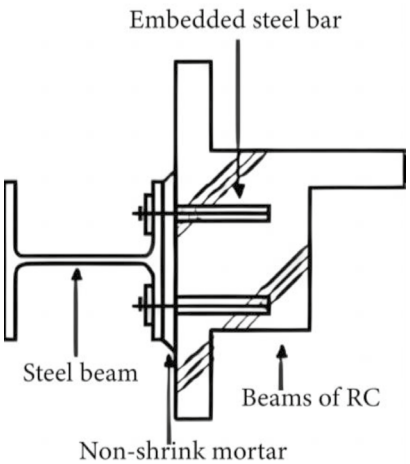

(c) Arrangement of post-installed rebar

Fig. 1 RC structural reinforcement project

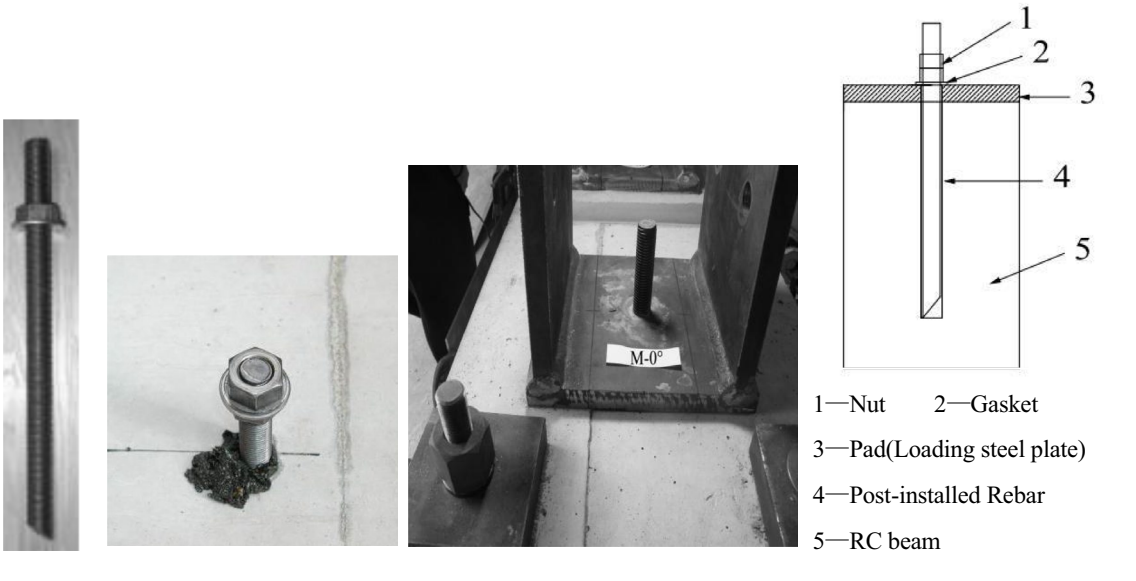

Fig. 2 Anchorage with post-installed rebar

Table 1 Test parameters

Specimens No	①	②	③	④	⑤	⑥	⑦
Name	C-90°	C-90°-0.7	M-90°	M-90°-0.7	M-60°	M-30°	M-0°
Load combination	Shear	Shear and 0.7 × t_u	Shear	Shear and 0.7 × t_u	Shear and tension	Shear and tension	Tension
Loading method	Repeatedly	Repeatedly	Uniaxial	Uniaxial	Uniaxial	Uniaxial	Uniaxial

Table 2 Mechanical properties of post-installed bars

Type	Yield stress σ_y (N/mm^2)	Tensile stress σ_u (N/mm^2)	Yield ratio yr (%)	Elongation el (%)
Post-installed rebar	335	520	63	20

3.2 Instrumentation

The locations of dial gauges are shown in Fig. 4a, b, it is similar to Fu and Parke (2018), Gao et al. (2017), Wang et al., (2020). In the test, the shear deformation and vertical deformation of the post-installed bar and the rotation of the loaded steel tool were detected through the RC beam fixed by the post-installed bar and the loaded steel plates. It consists of dial gauge for measuring horizontal displacement of the beam (*a*, *b*) and relative vertical displacement (*c*, *d*), anchorage shear deformation, relative vertical displacement between steel plates and RC beams (gauge *e*, *f*).

4 Test Results

4.1 Failure Modes

The load and deformation relationships of each specimen are shown in Fig. 5. Fig. 5a, c presents the deformation under cyclic loading, and Fig. 5b, d presents the deformation under unidirectional loading. The cordinate is tension (T) or vertical deformation (δ_V), and the horizontal coordinates is shear (V) or shear deformation (δ_H). In Fig. 5, the numbers ① ~ ⑦ represent the specimen which was classified in Table 1 with different load angles, load combinations and load methods.

In Fig. 5a, c, the specimen ① is mainly subjected to horizontal shear. The maximum load and shear deformation in eastward direction are 65.5 kN and 4.03 mm, respectively, while the maximum cyclic load and shear deformation in the westward direction are 47.8 kN and 4.0 mm, respectively. During the fabrication process,

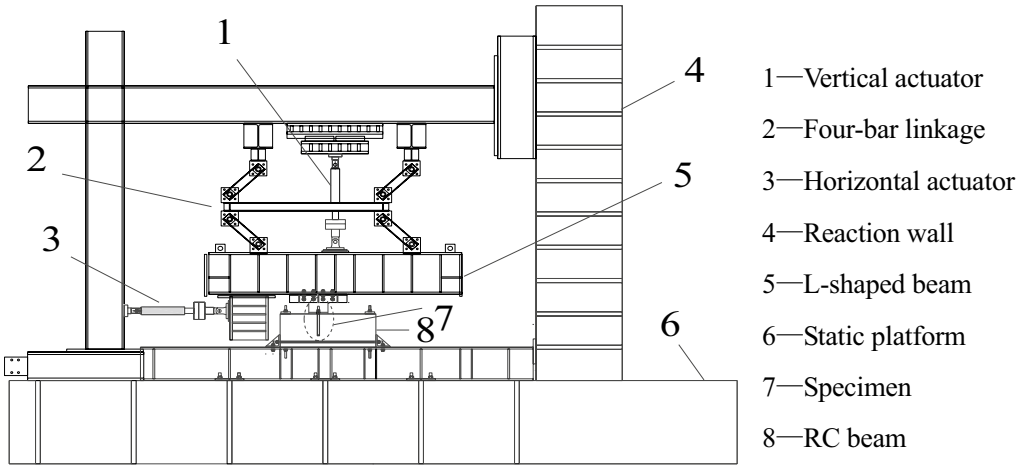

Fig. 3 Test rigs

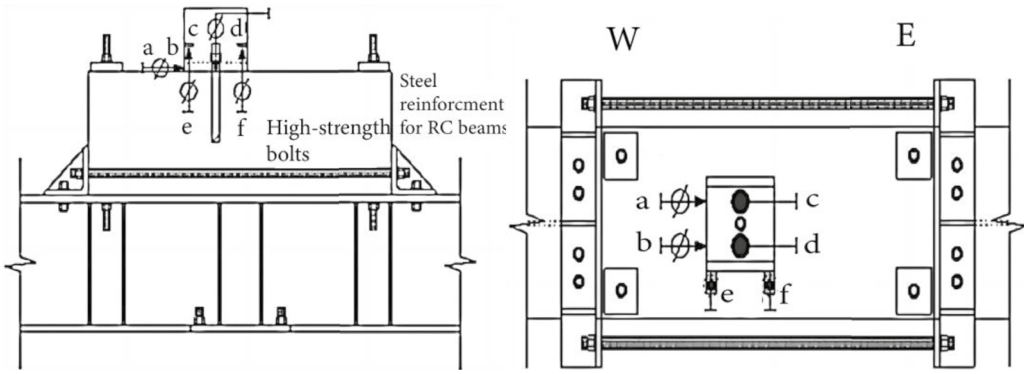

(a) elevation view of the location of dial gauge (b) plan view of the location of dial gauge

Fig. 4 Arrangement of dial gauge

defaults was made for the contact surface of the loading, causing the different in the positive and negative loading process, therefore the difference between the positive (65.6 kN) and negative (47.8 kN) bearing capacity of specimen ①.

When monotonic load (Fig. 6a) was applied on the beam, the final load, shear deformation and vertical deformation are 108.7 kN, 16.6 mm and 1.6 mm, respectively. The shear failure of the post-installed rebar is shown in Fig. 6b. For specimen ②, at 60 kN, the shear force and shear deformation in eastward direction are 29.5 kN and 4.0 mm, and in westward direction, the shear force and shear deformation are 36.5 kN and 4 mm under cyclic load; after monotonic loading was applied on the beam (Fig. 5c), the specimen with the shear deformation of 21 mm is shown in Fig. 6c; the ultimate load, shear deformation and vertical deformation in the final state are 70.5 kN, 26.5 mm and 9.9 mm, respectively; the shear failure of the post-installed bar is shown in Fig. 6d.

Specimens ③~⑦ in Fig. 5b, d were loaded under monotonic load, it can be seen that specimen ③ was mainly subjected to horizontal shear, the maximum load and shear deformation are 120 kN and 16.8 mm, respectively, and the post-installed bar shows shear failure. For specimen ④, the maximum shear load, the maximum shear deformation, vertical direction are 70 kN, 30 mm, 12 and 4 mm, respectively; the moments of deformation bifurcation at the east and west edges of specimen ④ are shown in Fig. 6e, and the final shear failure of the post-installed rebar is shown in Fig. 6f. Specimen ⑤ was subjected to both shear and tensile forces. The shear deformation and vertical deformation of specimen ⑤ are similar to those of specimen ③, and the post-installed rebar shows shear failure. The specimen ⑥ was in combined tension and shear. The maximum tensile force is 120 kN and the shear force is 60 kN at the same time; vertical cracks occurred in the RC beam during the test, as shown in Fig. 6g, but the specimen also eventually

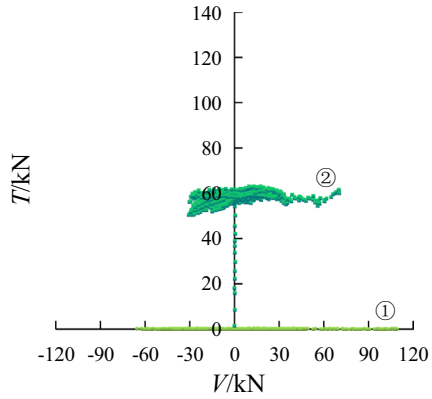

(a) *T-V* of specimen ① and ②

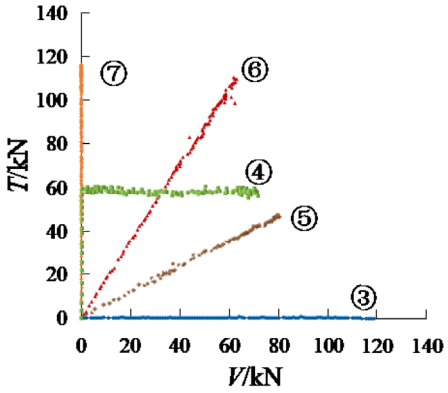

(b) *T-V* of specimen ③~⑦

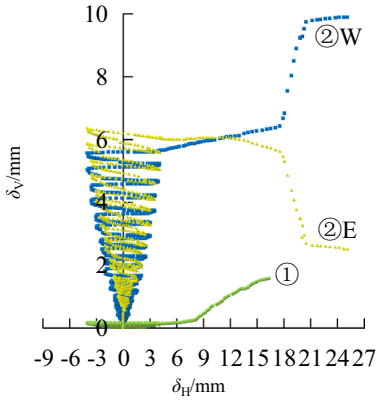

(c) δ_V - δ_H of specimen ① and ②

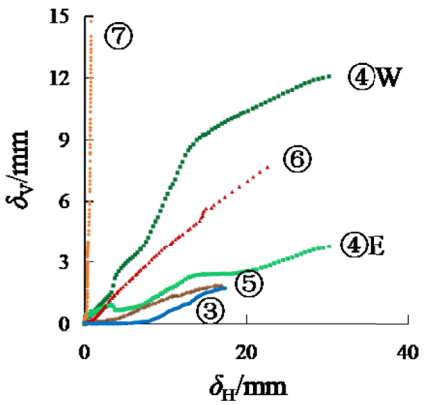

(d) δ_V - δ_H of specimen ③~⑦

Fig. 5 load and deformation relationship of each specimen

failed in shear. specimen ⑦ was in tension. In the experiment, the RC beam had vertical cracks, and finally the post-installed rebar pulled out. The concrete cone around the post-installed rebar is shown in Fig. 6h.

It can be seen from above test results that under different loading conditions of the same specimen, the load bearing and deformation capacities are different. The specimens ① and ③ under only shear force have larger shear capacity compared to the remaining specimens; when the specimens are under the combined action of shear and tension, the shear capacities of the specimens become smaller, and the deformation capacities increase with increasing tension force.

4.2 The Load–Deformation Relationship of the Specimen

4.2.1 Cyclic Load

The shear force–deformation curves of specimens ① and ② are shown in Fig. 7. Under low-cycle loading, for Specimen ①, the maximum load generated in the westward direction is 47.8 kN with 1 mm shear deformation for the first cycle. With the increase of the number of cycles, the shear capacity of the specimen reduces; when shear deformation is over 3 mm, the shear capacity of the specimen is gradually increased. The maximum load and shear deformation in the eastward direction are 65.5 kN and 4.03 mm. The yield shear force of specimen ① is 45 kN, and the shear force and shear deformation at failure are 10 9 kN and 16.6 mm.

Under low-cycle loading, for Specimen ②, the shear deformation is between − 1.5 and 1.5 mm. The carrying capacity is gradually increased within the range in the positive and negative for 1.5 mm maximum load carrying capacity of the shear deformation of the first return 36.5 kN, yielding The shear force is 20 kN; when the absolute value of the shear deformation is greater than 1.5 mm, the bearing capacity of specimen ② gradually decreases. Under cyclic loading, the hysteresis curve of test piece ② is slipping. After the loading is changed from repeated

(a) loading of specimen ①

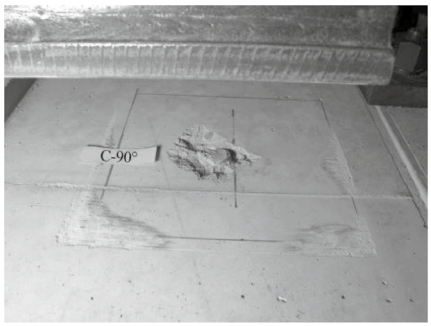

(b) failure mode of specimen ①

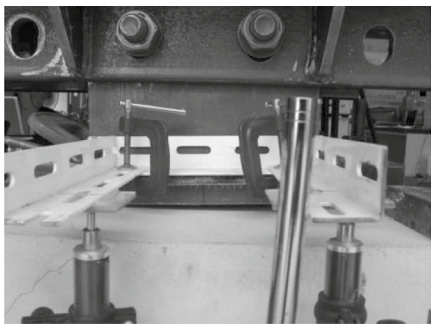

(c) Specimen ② at shear deformation of 21mm

(d) failure mode of specimen ②

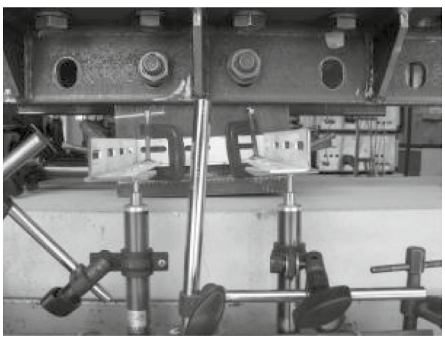

(e) the moments of deformation bifurcation at the east and west edges of specimen ④

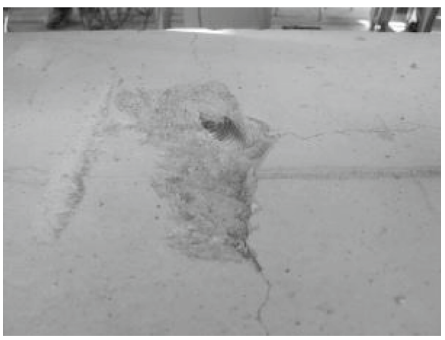

(f) failure mode of specimen④

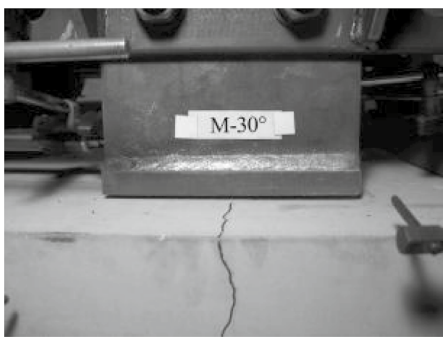

(g) Cracking in specimen ⑥

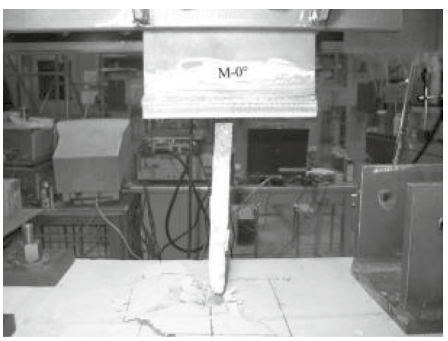

(h) failure mode of specimen⑦

Fig. 6 Failure modes of specimens

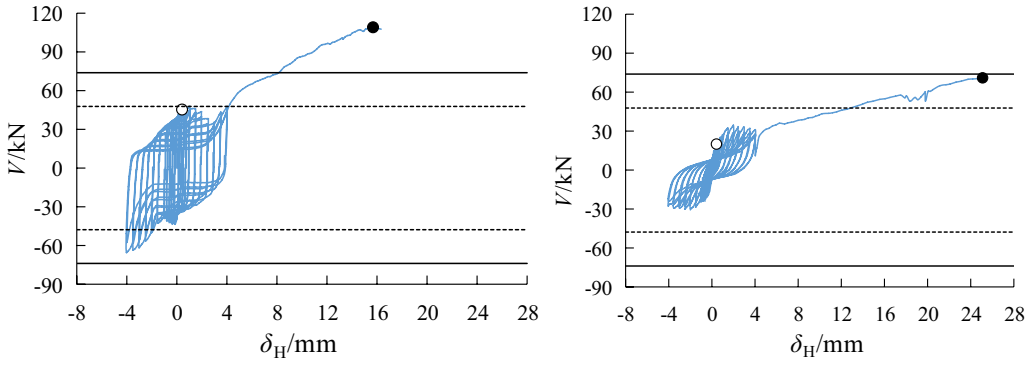

(a) V-δ_H of specimen ① (b) V-δ_H of specimen ②

Fig. 7 The Shear–deformation curve

to monotonic loading, the shear deformation and bearing capacity of specimen ② increase simultaneously, and the shearing force and shear deformation when the post-installed rebar fails are 70.5 kN and 26.5 mm.

Under cyclic loading, the energy dissipation performance of post-installed bar under a single shear load is stronger than the energy dissipation performance of the combined shear and tensile load.

4.2.2 Monotonic Load

Fig. 8a shows the relationship between shear force (V) and shear deformation (δ_H) of specimen ③ ~ ⑥. Fig. 8b shows the relationship between the tensile force (T) and tensile deformation (δ_V) of specimen ④ ~ ⑦.

From the relationship between the shear force (V) and shear deformation (δ_H) of specimens ③ ~ ⑥, it can be concluded that, with the increase of the slop, the yield shear force, maximum shear force, initial stiffness and second stiffness of the specimen also increase, but the maximum shear deformation tends to decrease. In addition, as the angle between the post-installed rebar and the force increases, the shear force of the same shear deformation decreases.

For the specimen ④ subjected to the coupling action of tensile force and shear force, the values of yield shear force, initial stiffness and second stiffness are smaller than other specimens, and the shear deformation is larger than other specimens. In addition, when the shear deformation is ≤ 8 mm, the shear force of specimen ④ is the smallest; when the shear deformation is > 8 mm, the shear force is greater than that of specimen ⑥ and less than that of other specimens.

From the tensile deformation (δ_V) relationship of specimens ④ ~ ⑦ tension (T) it can be seen with the increase of the slop, the tensile force of the same tensile deformation becomes smaller, the yield tensile force and the maximum tensile force of the specimen become smaller, and the maximum tensile deformation becomes smaller.

For specimens ④ subjected to the coupling effect of tension and shear forces, the yield tension value is greater

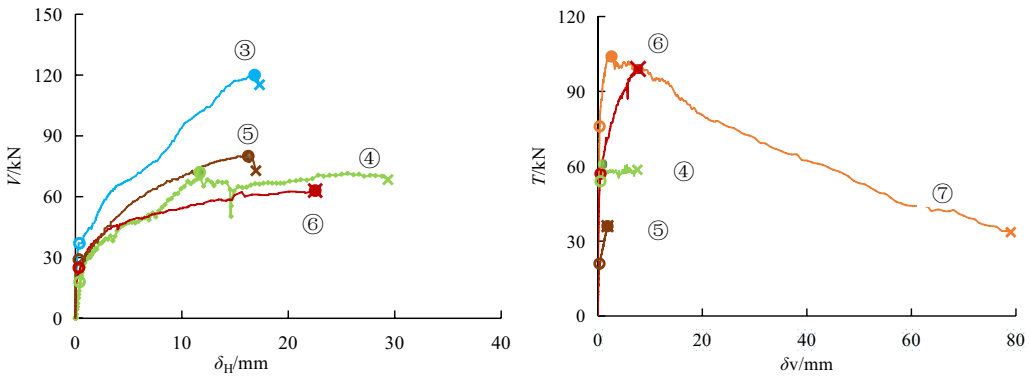

(a) V-δ_H of specimen ③~⑥ (b) T-δ_V of specimen ④~⑦

Fig. 8 The Load–deformation curve

than specimen ⑤ and ⑥ and smaller than specimen ⑦; while the maximum tensile value is greater than specimen ⑤ and smaller than specimens ⑥ and ⑦. Due to the influence of the force characteristics, specimen ④ can bear a large tensile force of 60 kN within a small deformation of 0.3 mm.

Based on the test results of specimens ③ ~ ⑦, it can be seen that the initial stiffness, yield load, maximum load and maximum deformation of specimens ③ and ④ with different loading methods are similar. For different angles between the post-installed rebar and the loadings of each specimen (0°, 30°, 60°, and 90°). The specimen with an included angle of 0° ⑦ is pulled out by unidirectional tension; The specimens ③ with an included angle of 90° are subjected to unidirectional shear force and shear failure of the post-installed rebar occurred; For specimens ④, ⑤ and ⑥ which are subjected to the coupling action of shear and tensile force, as the angle increases, the shear performance (yield shear, maximum shear, and initial stiffness) of each specimen increases, while the tensile performance (yield tension, maximum tension, and initial stiffness) decreases.

5 Design Formula of Anchor Bolt

The strength of anchor bolt is calculated based on the design formula of from codes in China, the United States and Japan. The design formula of anchor bolt strength under combined shear–tension in Chinese code (Ministry of Housing & Urban-Rural Development, 2013) is

$$\left(\frac{N_{sc}}{0.77N_y}\right)^2+\left(\frac{V_{sc}}{0.39V_y}\right)^2=1 \tag{1}$$

The strength design formula of anchor bolts under shear–tension coupling in American code (AISC360—16, 2016):

$$\left(\frac{N_{su}}{0.75N_u}\right)^{5/3}+\left(\frac{V_{su}}{0.65V_u}\right)^{5/3}=1 \tag{2}$$

The design formula of anchor bolt strength under shear–tension coupling in Japanese standard (Design Recommendations for Composite Constructions, 2010):

$$\left(\frac{N_{sj}}{N_u}\right)^2+\left(\frac{V_{sj}}{0.7V_u}\right)^2=1 \tag{3}$$

In the above formulas (1)–(3): N_{sc}, N_{su} and N_{sj} are the design tensile force of the post-installed bar, V_{sc}, V_{su} and V_{sj} are the design shear force of post-installed bar.

It can be seen from Table 3, the Chinese code formula is the most conservative, as it is based on the yield force of the bolt. The maximum load-bearing capacity of the bolt test designed with the American and Japanese codes is based on the maximum load of the anchor bolt, which is also conservative compared to the test results; the theoretical value of the Japanese code is closest to the test value. The ultimate capacity of the concrete structure after retrofitting is higher than the theoretical value from the code; for example, the maximum load-bearing capacity of specimen ③ is 2.27 times of the theoretical value of the American code and 2.06 times the theoretical value of the specification of Japan.

6 Shear-Resistant of the Post-installed Rebar

6.1 Equivalent Shear Capacity Analysis

Through the test, we can investigate the external situation of the test of the post-installed rebar, and it is difficult to predict the mechanism of the stress, strain distribution, the interplay between the post-installed rebar, the Cementitious material and concrete.

To further clarify the shear mechanism of the post-installed rebar, the interaction relationship between the post-installed rebar and the cementing material and concrete is assumed. In Fig. 9a, the shear force of the cementitious material and concrete is V, and the shear force V and the cementing material and concrete react on the local pressure balance of the post-installed rebar. Section pressure of the reinforcement under monotonic shear force is uneven distributed, as left in Fig. 9b; to calculate the evenly distributed pressure stress (σ_{cc}) acting on diameter (d), Fig. 9b, right, ($\sigma_{cc}=3\sigma_{cy}$) (Liu et al., 1985); pressure area of the reinforcement ($h\cdot d$), Fig. 9c. In Fig. 9a, the shear force of the bolt in the RC beam (point C) is zero, the distance between point C and RC beam top point B is h; the spacing between

Table 3 Test and theoretical value of specimens' strength (unit: kN)

Specimens No	①	②	③	④	⑤	⑥	⑦
V_u (T_u)	109	71 (63)	120	72 (61)	80 (36)	63 (99)	(104)
V_y (T_y)	45	20 (56)	37	18 (57)	29 (21)	25 (54)	(76)
V_{sc} (N_{sc})	21		21		20	18 (20)	(41)
V_{su} (N_{su})	53		53		49 (20)	31 (45)	(62)
V_{sj} (N_{sj})	58	38 (63)	58	39 (61)	56 (24)	41 (60)	(83)

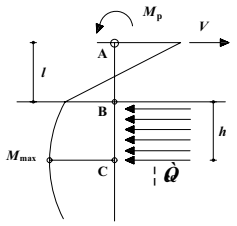

(a) Interaction of the post-installed rebar with Cementitious material and concrete

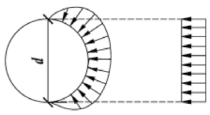

(b) monotonic shear pressure of the post-installed rebar

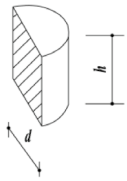

(c) pressure area of the post-installed rebar

Fig. 9 Capacity of the post-installed rebar specimen

points B and A on the reinforcement (l), l=30 mm when the steel is directly fixed on the beam.

Equation (4) shows when the reinforcement is in synergy with the Cementitious material and concrete:

$$V = \sigma_{cc} \cdot h \times d \tag{4}$$

When the moment action at both point A and C of the post-installed rebar reaches the plastic moment of the full cross section of the implant, the equation for the moment balance at point C is Eq. (5):

$$M_p = -M_p + V(l+h) - \int_0^h \sigma_{cc} \cdot d \cdot (h-x)\mathrm{d}x \tag{5}$$

Equation (6) is obtained from Eq. (5):

$$M_p = -M_p + V \cdot l + \frac{V \cdot h}{2} \tag{6}$$

The plastic moment of the full cross section of the post-installed rebar when axial action is not considered is given by the following equation:

$$M_p = f_y \cdot \frac{\pi \cdot d^3}{32} \tag{7}$$

Substitute Eqs. (4) into (6) for the unknown quantity h:

Table 4 Relationship of V_{max} and ${}_tV_y$

Specimen number	${}_tV_y$/kN	V_{max}/kN	${}_tV_y/V_{max}$
T-①	35.8	15.4	2.33
T-②	31.3	15.4	2.03
T-③	45.3	44.1	1.03
T-④	37.1	44.1	0.84

$$M_p = -M_p + \sigma_{cc} \cdot h \cdot d \cdot l + \frac{\sigma_{cc} \cdot h \cdot d \cdot h}{2} \tag{8}$$

$$\sigma_{cc} \cdot d \cdot h^2 + 2 \cdot \sigma_{cc} \cdot d \cdot l \cdot h - 4M_p = 0 \tag{9}$$

$$h^2 + 2 \cdot l \cdot h - 4M_p/\sigma_{cc} \cdot d = 0 \tag{10}$$

$$h = -l \pm \sqrt{l^2 + \frac{4M_p}{\sigma_{cc} \cdot d}} \tag{11}$$

h denotes height and h is Eq. (11):

$$h = -l + \sqrt{l^2 + \frac{4M_p}{\sigma_{cc} \cdot d}} \tag{12}$$

Equation (12) is substituted into Eq. (4) for the equivalent shear bearing capacity V_{max}:

$$V_{max} = \sigma_{cc} \cdot d \cdot (-l + \sqrt{l^2 + \frac{4M_p}{\sigma_{cc} \cdot d}}) \tag{13}$$

The V_{max} values of the implant specimens and the tested yield shear ${}_tV_y$ of specimens T-① to ④, calculated based on Eq. (13), are shown in Table 4.

As can be seen from Table 4, for specimens T-①~② with mortar bedding, the deviations between the calculated and measured results are large; the mortar bedding is considered as void in the calculation, which is not consistent with the actual working conditions; therefore, the equivalent bearing capacity (V_{max}) value is less than the yield shear force ${}_tV_y$. The calculated values of specimens T-③~④ are in good agreement with the measured results, and the concrete structure without mortar bedding can be better judged by the above method. The yield strength of the connection.

7 Conclusion

Through the above research and comparative analysis, the conclusions are drawn as follows:

(1) As the angle between the post-installed bar and the applied force becomes larger, the shear force and shear stiffness of the specimen will also increase; while the tensile force and tensile stiffness of the specimen decrease, and the maximum shear deformation and maximum tensile deformation also decrease.
(2) The loading method has no significant effect on the strength and stiffness of the specimen, and the bearing capacity and stiffness of the specimen under a single load are greater than those under coupled load. The concrete located at the post-installed rebar exhibits conical failure when the post-installed rebar of the specimen subjected to a single tensile force is pulled out. The post-installed rebar for other specimens is the shear failure. The maximum bearing capacity of the specimens is greater than the theoretical value specified in the specifications, especially when subjected to single loading, which is much greater than the theoretical value specified in the specifications.
(3) When the shear load is predominant, the theoretical value of the equivalent shear capacity of the specimen is close to the yield shear force, and the theoretical value of the equivalent tensile capacity of each specimen is consistent with the maximum bearing tensile force.

Acknowledgements
This research was financially supported by National Natural Science Foundation of China (Grant NO., 51968013), National Natural Science Foundation of Guangxi (Grant NO., 2022GXNSFAA035529). The authors wish to acknowledge the sponsors. However, any opinions, findings, conclusions and recommendations presented in this paper are those of the authors and do not necessarily reflect the views of the sponsors.

Author contributions
RZ: conceptualization, methodology, supervision reviewing and editing. EHB: supervision data curation, XY: visualization, investigation. FF: supervision writing—original draft preparation. Writing—reviewing and editing.

Funding
National Natural Science Foundation of China (Grant NO., 51968013), National Natural Science Foundation of Guangxi (Grant NO., 2022GXNSFAA035529).

Availability of data and materials
The data and materials used to support the findings of this study are available from the authors upon request.

Declarations

Ethics approval and consent to participate
Not applicable.

Consent for publication
All authors consent for publication.

Competing interests
The authors declare that they have no known competing financial interests or personal relationships that could have appeared to influence the work reported in this paper.

Received: 4 November 2023 Accepted: 20 May 2024
Published online: 20 September 2024

References

ACI318—11 Building Code Requirements for Structural Concrete and Commentary. American Concrete Institute, 2013.
AISC360—16, Specifications for Structural Steel Buildings[S]. American Institute of Steel Construction, 2016.
Çalışkan, Ö., Yılmaz, S., Kaplan, H., & Kıraç, N. (2013). Shear strength of epoxy anchors embedded into low strength concrete. *Construction and Building Materials, 38*(2), 723–730.
Cheng, L., Jiansheng, F., & Jianguo, N. (2017). Fatigue performance research of headed studs in steel and ultra-high performance concrete composite deck. *China Journal of Highway and Transport, 30*(3), 139–146.
Civil and Structural Groups of Tsinghua University, Xian Jiaotong University and Beijing Jiaotong University. (2008). Analysis on seismic damage of buildings in the Wenchuan earthquake. *Journal of Building Structures*, *29*(4), 1–9.
Design Recommendations for Composite Constructions. Architectural Institute of Japan, 2010.
Ding, H., Guo, Y., Liang, Y., & Zhang, P. (2016). Experimental research on seismic performance of storey-adding frame structures. *Transactions of Tianjin University, 22*(1), 43–49.
Fu, F., & Parke, G. A. R. (2018). Assessment of the progressive collapse resistance of double-layer grid space structures using implicit and explicit methods. *International Journal of Steel Structures, 18*(3), 831–842.
Gao, S., Guo, L., Fu, F., & Zhang, S. (2017). Capacity of semi-rigid composite joints in accommodating column loss. *Journal of Constructional Steel Research, 139*, 288–301.
Gesoğlu, M., Güneyisi, E. M., Güneyisi, E., Yılmaz, M. E., & Mermerdaş, K. (2014). Modelling and analysis of the shear capacity of adhesive anchors post-installed into uncracked concrete. *Composites, Part b: Engineering, 60*(1), 716–724.
Jianguo, N., Yixin, Li., & Muxuan, T. (2014). Slip performance and hysteresis model of a new type of uplift restricted-slip free connectors. *Engineering Mechanics, 31*(11), 46–52.
Lee, J., Goldsworthy, H. M., & Gad, E. F. (2010). Blind bolted T-stub connections to unfilled hollow section columns in low rise structures. *Journal of Constructional Steel Research, 66*(8/9), 981–992.
Liu, C., Yu, J., Lu, Z., & Wang, K. (2010). Experimental study on bond-slip behavior of post-installed rebar at high temperature. *Journal of Tongji University, 38*(11), 1579–1585.
Ministry of Housing and Urban-Rural Development, People's Republic of China. JGJ145—2004 Technical specification for post-installed fastenings in concrete structures. China Architecture & Building Press, 2005.
Ministry of Housing and Urban-Rural Development, People's Republic of China. GB50011—2010 Code for seismic design of building. China Architecture & Building Press, 2010.
Ministry of Housing and Urban-Rural Development, People's Republic of China. JGJ145—2013 Technical specification for post-installed fastenings in concrete structures. China Architecture & Building Press, 2013.
Mourad, S. (1993). *Behaviour of blind bolted moment connections for square HSS columns*. Memaster University.
Mourad, S., Korol, R. M., & Ghobarah, A. (1996). Design of extended endplata connections for hollow section columns. *Canadian Journal of Civil Engineering, 23*(1), 277–286.
Nie, J. G., Li, Y. X., Tao, M. X., & Nie, X. (2015). New technique and application of uplift-restricted and slip-permitted connection. *China Civil Engineering Journal, 48*(4), 7–14.

Peng, H., Liu, D. W., Dai, B., Zeng, S. S., & Chu, F. J. (2018). Experimental research on load-shear performance of interface between new and old concrete with corroded post-installed bar. *Chinese Journal of Engineering, 40*(1), 23–30.

Qian, K., Geng, S. Y., Liang, S. L., Fu, F., & Yu, J. (2022). Effects of loading regimes on the structural behavior of RC beam-column sub-assemblages against disproportionate collapse. *Engineering Structures, 251*, 113470.

Qian, K., Liang, S. L., Feng, D. C., Fu, F., & Wu, G. (2020). Experimental and numerical investigation on progressive collapse resistance of post-tensioned precast concrete beam-column sub-assemblages. *Journal of Structural Engineering, 146*(9), 04020170.

Qian, K., Weng, Y. H., Fu, F., & Deng, X. F. (2021). Numerical evaluation of the reliability of using single-story substructures to study progressive collapse behaviour of multi-story RC frames. *Journal of Building Engineering, 33*, 101636.

Wang, L., Shen, N., Zhang, M., Fu, F., & Qian, K. (2020). Bond performance of Steel-CFRP bar reinforced coral concrete beams. *Construction and Building Materials, 245*, 118456.

Xiaosong, R., Xianyu, W., Bin, Z. (2018). Experimental study on seismic behavior of post-installed reinforced concrete-masonry composite wall connected with embedded bars. *Journal of Building Structures, 39*(4), 45–53.

Xie, G. H., Liu, R. G., Chen, B., Li, M. J., & Shi, T. G. (2015). Synergistic effect of a new wedge-bond-type anchor for CFRP tendons. *Journal of Central South University, 22*(6), 2260–2266.

Yilmaz, S., Özen, M. A., & Yardim, Y. (2013). Tensile behavior of post-installed chemical anchors embedded to low strength concrete. *Construction and Building Materials, 47*(5), 861–866.

Zhang, Y., Lou, G., Li, G., et al. (2016). Experimental study of bond strength of anchorage adhesive after heating. *Journal of Tongji University, 44*(11), 1723–1728.

Publisher's Note

Rong Zeng PhD, Associate Professor, Guangxi Key Laboratory of Green Building Materials and Construction Industrialization, Guilin University of Technology, China, 541004

En-He Bao PhD, Professor, Guangxi Key Laboratory of Green Building Materials and Construction Industrialization, Guilin University of Technology, China, 541004

Xia Yin PhD, Associate Professor, Guangxi Key Laboratory of Green Building Materials and Construction Industrialization, Guilin University of Technology, China, 541004

Feng Fu PhD, Associate Professor Department of Engineering, School of Science & Technology, City, University London, Northampton Square, London, UK, EC1V0HB: Adjunct Professor, Guangxi Key Laboratory of Green Building Materials and Construction Industrialization, Guilin University of Technology, China, 541004